

Polycube Layouts via Iterative Dual Loops

MAXIM SNOEP, TU Eindhoven, The Netherlands
 BETTINA SPECKMANN, TU Eindhoven, The Netherlands
 KEVIN VERBEEK, TU Eindhoven, The Netherlands

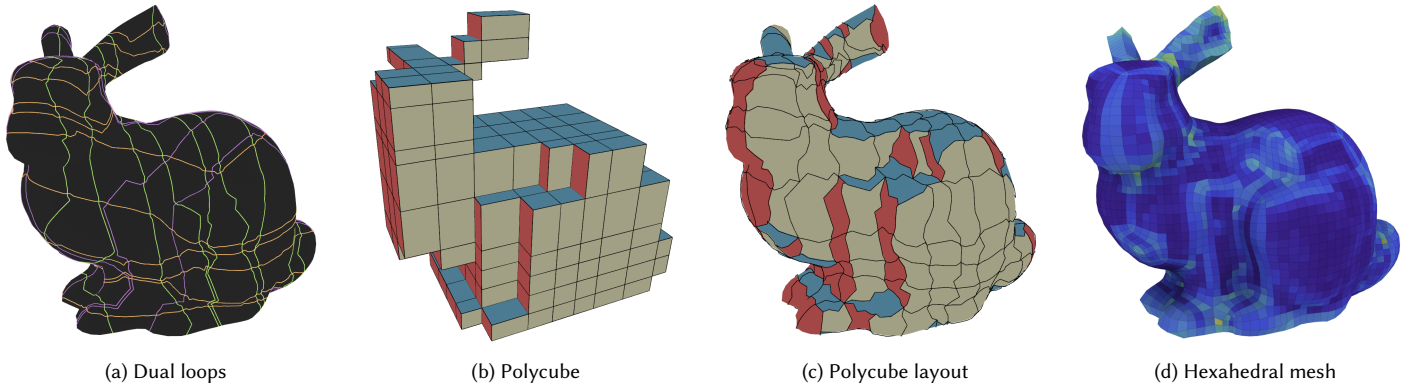


Fig. 1. An iterative approach for the computation of polycube layouts using the dual loop structure of polycubes.

ABSTRACT

Polycube layouts for 3D models effectively support a wide variety of applications such as hexahedral mesh construction, seamless texture mapping, spline fitting, and multi-block grid generation. However, the automated construction of valid polycube layouts suffers from robustness issues: the state-of-the-art deformation-based methods are not guaranteed to find a valid solution. In this paper we present a novel approach which is guaranteed to return a valid polycube layout for 3D models of genus 0. Our algorithm is based on a dual representation of polycubes; we construct polycube layouts by iteratively adding or removing dual loops. The iterative nature of our algorithm facilitates a seamless trade-off between quality and complexity of the solution. Our method is efficient and can be implemented using comparatively simple algorithmic building blocks. We experimentally compare the results of our algorithm against state-of-the-art methods. Our fully automated method always produces provably valid polycube layouts whose quality – assessed via the quality of derived hexahedral meshes – is on par with state-of-the-art deformation methods.

1 INTRODUCTION

Polycubes, or orthogonal polyhedra, are polyhedra with axis-aligned quadrilateral faces. Their simple structure enables efficient solutions to various challenging geometric problems. Bijective mappings of general shapes to polycubes, so-called *polycube maps*, are used to transfer solutions computed on polycubes into more general settings. In this manner, polycube maps are used to solve problems such as texture mapping [Tarini et al. 2004] and interior hexahedral

meshing [Pietroni et al. 2022]. The latter is currently the dominant application area for polycube maps, to a degree that the quality of the final interior hexahedral mesh is used to assess the quality of the polycube map from which it is derived.

More formally, a polycube map is a map between the surface of a polycube Q and the surface mesh of a 3D model M . The image of the quadrilateral faces of Q segments M into so-called *patches*. Each patch has exactly four neighbors and a *label* $\pm X/\pm Y/\pm Z$: the direction of the normal vector of its corresponding polycube face. This segmentation into patches is called a *polycube layout*.

Polycube layouts are related to *polycube labelings* or *polycube segmentations*. A polycube labeling (or polycube segmentation) is defined as an assignment of the labels $\pm X/\pm Y/\pm Z$ to each face of the surface mesh M . Adjacent faces with the same label form a *chart*. Charts are similar to the patches of polycube layout; both are subsurfaces of M sharing a single label. However, in a polycube labeling a chart is exclusively adjacent to charts with different labels, and its number of neighbors is unrestricted. In a polycube layout a patch is adjacent to exactly four other patches, and these patches may have the same label. To construct a polycube labeling from a polycube layout one can assign the label of each patch to the mesh faces inside the patch. Conversely, to construct a polycube layout from a polycube labeling one can divide each chart into conforming quadrilateral patches.

Since polycube maps were introduced in 2004, a variety of methods have been proposed to construct them. The quality of a polycube

map is determined by two factors: the complexity of the polycube and the distortion introduced by the mapping. All methods that construct polycube maps must find a balance between these conflicting factors. The state-of-the-art achieves a good trade-off between low distortion and low complexity by using deformations [Dumery et al. 2022; Gregson et al. 2011; Livesu et al. 2013]. However, current deformation-based methods suffer from robustness issues since none can guarantee that the polycube labelings they construct are valid [Mestrallet et al. 2023; Protais et al. 2022; Sokolov and Ray 2015; Zhao et al. 2019]. Furthermore, current techniques that check the validity of labelings are limited [Mestrallet et al. 2023]; they incorrectly identify invalid labelings as valid, and vice-versa. Some of these validation checks are based on the characterization of orthogonal polyhedra by [Eppstein and Mumford 2010] and as such restricted to polycubes with corners of degree three or four.

We present a novel approach which is guaranteed to return a valid polycube layout for 3D models of genus 0. Our method builds upon a combinatorial characterization of polycubes of genus 0 in a dual representation [Baumeister and Kobbelt 2023]. We construct polycube layouts from an initial valid layout (a single cube) to which we add and subtract additional cubes via their representation as loops in the dual. It follows directly from the combinatorial characterization that we maintain a valid layout at each point during our iterative construction. Furthermore, we prove that we can always add loops (layers of cubes) between any two existing loops. The iterative nature of our algorithm allows us to explicitly control the trade-off between the complexity of the polycube and the distortion introduced in the mapping. As it is common in the current literature, we assess the quality of our polycube maps via the quality of interior hexahedral meshes derived from them via a state-of-the-art meshing pipeline. Our fully automated method always produces provably valid polycube layouts whose quality is on par with state-of-the-art deformation methods.

We review related work in Section 2 and give the necessary mathematical background, including the dual representation of polycubes in Section 3. We present our iterative algorithm that constructs provably valid polycube layouts in Section 4. We report on experimental results in Section 5 and conclude with a discussion in Section 6.

2 RELATED WORK

In 2004 [Tarini et al. 2004] introduced polycube maps as an extension of cube maps. Since polycube maps proved to be an effective tool to solve challenging problems such as hexahedral meshing, many methods have been proposed to automate their construction. The first methods by [Tarini et al. 2004] and [Wang et al. 2008] constructed polycube maps from manually constructed polycubes. The first fully automatic polycube construction methods had significant drawbacks, as they produced polycubes that were either very coarse [Lin et al. 2008] or very detailed [He et al. 2009].

The most prominent methods for polycube construction are based on the deformation approach by [Gregson et al. 2011] which was later improved or extended by many [Cherchi et al. 2016; Dumery et al. 2022; Fang et al. 2016; Fu et al. 2016; Guo et al. 2020; Huang et al. 2014; Livesu et al. 2013; Mandad et al. 2022; Yang et al. 2019; Yu et al. 2014; Zhao et al. 2019]. The deformation-based approaches

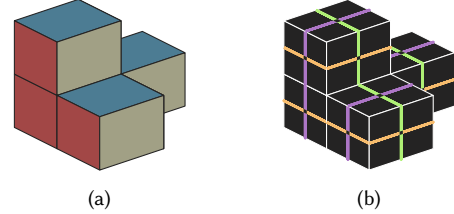


Fig. 2. A polycube (a) its dual representation (b); loops of type $X/Y/Z$ (green/orange/purple).

find an initial polycube labeling in various ways, none of which guarantees that the labeling corresponds to a valid polycube. Then, the input shape is gradually deformed until the surface faces are oriented toward their assigned target label. The initial polycube labeling may be adjusted during the deformation process. Many deformation methods use the characterization of orthogonal polyhedra by [Eppstein and Mumford 2010] to increase their robustness, however, this characterization is neither sufficient nor necessary for valid polycubes [Mandad et al. 2022; Mestrallet et al. 2023; Pietroni et al. 2022; Sokolov and Ray 2015].

An alternative set of methods is based on voxelization [Wan et al. 2011]. Voxelization may be used in combination with deformation to guarantee valid solutions [Yang et al. 2019; Yu et al. 2014]. However, voxelization results in overly detailed polycubes, which is not desirable for most downstream applications.

[Biedl and Genc 2004] characterized orthogonal convex polyhedra (a subset of all polycubes) via a dual representation. Nearly 20 years later, [Baumeister and Kobbelt 2023] independently derived a fully combinatorial dual characterization of all polycubes of genus 0. These dual representations are a collection of labelled loops corresponding to the $X/Y/Z$ directions (see Fig. 2). Based on their characterization, [Baumeister and Kobbelt 2023] propose a method to construct polycubes via loop structures extracted from quadrilateral meshes obtained from [Campen et al. 2012]. However, these loop structures do not necessarily correspond to polycubes and hence they use a local search to find a valid polycube representation. This search is purely combinatorial and disregards the geometry of the input mesh. Therefore the resulting polycubes are frequently not similar to the input and have a large mapping distortion. In contrast, we use the dual characterization directly and iteratively construct a valid dual loop structure on the input mesh, while considering geometric features and mapping distortion.

3 POLYCUBES AND THEIR DUAL STRUCTURE

Our input is a 3D model represented by a triangulated surface mesh $\mathcal{M} = (V, T)$, where V is the set of vertices and T is the set of triangular faces, each represented by a triple (v_i, v_j, v_k) of vertices. The edges of \mathcal{M} are represented implicitly via the triangles. We assume that \mathcal{M} is a genus 0 orientable manifold, that is, \mathcal{M} is homeomorphic to the sphere. Furthermore, we assume that \mathcal{M} is embedded in \mathbb{R}^3 , that every vertex $v \in V$ has an associated position $p(v)$, and that each triangle $t \in T$ has an associated normal $n(t)$.

A polycube Q is an orthogonal polyhedron with rectangular faces. The edges and normals of these faces are parallel to the axes

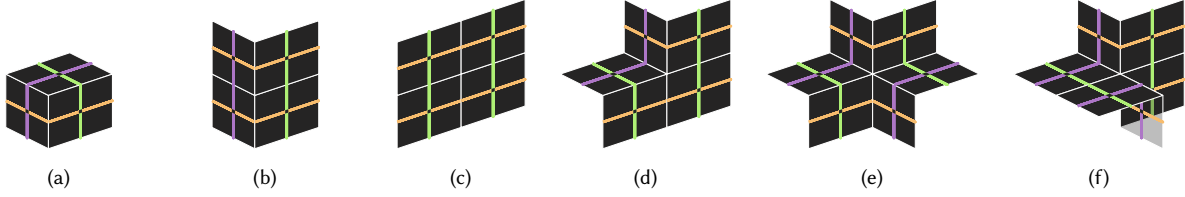


Fig. 3. The six possible combinatorial corner types of a polycube, characterized by the dual loops and dual faces of the polycube.

$\pm X/\pm Y/\pm Z$. A *polycube map* f is a bijective mapping between a polycube Q and a mesh \mathcal{M} . The image of the faces of Q induces a segmentation of \mathcal{M} , which is called a *polycube layout*. This polycube layout consists of *patches* corresponding to the faces of Q . Each patch has exactly four neighboring patches and is associated with the normal of its corresponding face in Q . Not every subdivision of a mesh into faces that have four neighbors and a normal is a *valid polycube layout*; valid polycube layouts correspond bijectively to a polycube. Our algorithm constructs only valid polycube layouts.

We can interpret a polycube Q as a collection of cubes glued together along complete faces. Consider a single *layer* L of cubes along the X -axis, that is, all cubes of Q that contain the same x -coordinate x_L . Layer L can consist of several connected components, if so, consider a single component C . The points on the surface of C which have x -coordinate x_L form a single closed loop around the cubes in C . We refer to such a loop as an X -loop of Q . There are infinitely many homotopic X -loops for each component C . We can choose an arbitrary X -loop to represent each component of each layer of Q ; we refer to the set of all representative X -loops by \mathcal{L}_X . Y - and Z -loops are defined correspondingly and the sets of all representative Y - and Z -loops are denoted by \mathcal{L}_Y and \mathcal{L}_Z (see Fig. 2). We refer to $\mathcal{S} = (\mathcal{L}_X, \mathcal{L}_Y, \mathcal{L}_Z)$ as the *loop structure* of the polycube Q . The loop structure \mathcal{S} of Q completely characterizes Q and serves as its dual representation. We hence refer to the representative X -, Y -, and Z -loops also simply as *dual loops*. Finally, we say that a loop structure \mathcal{S} is *valid* if it is the loop structure of a polycube.

Imagine now that we are cutting the polycube Q along the dual loops in \mathcal{L}_X . We refer to the resulting connected components as *zones* of type X (or type Y and Z , respectively). A zone is bounded by at least one dual loop and can be bounded by an arbitrary number of dual loops: consider a fork-like model with n teeth, the zone at

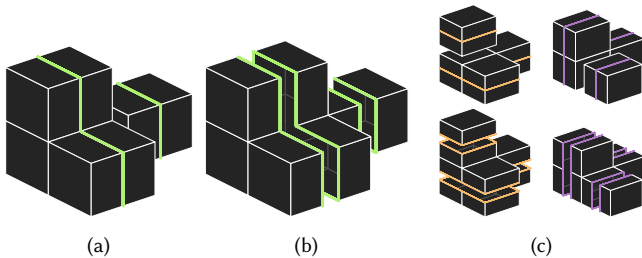


Fig. 4. The layers (a) and zones (b) defined by the X -loops. Similarly defined for the Y - and Z -loops (c).

the branching point is bounded by $n + 1$ loops. The regions bounded by the dual loops are called *dual faces* (see Fig 3).

The characterization of valid loop structures by [Baumeister and Kobbelt 2023] uses loops obtained via the quad meshes of [Campen et al. 2012] which have the property that no three loops intersect in one point. Below we repeat the characterization of [Baumeister and Kobbelt 2023], but make the implicit assumption on triple intersections explicit to arrive at the most general characterization.

A loop structure \mathcal{S} is valid (is the dual of a polycube) if:

- (1) Two loops of the same type ($X/Y/Z$) do not intersect;
- (2) No three loops intersect in the same point;
- (3) The dual faces are consistent with one of the six possible polycube corner-types, see Fig. 3. Specifically, the boundary of each dual face consists of between 3 and 6 distinct loops, and there are at most two loops of each type ($X/Y/Z$);
- (4) Let the *loop complex* of type X be the graph obtained by having a vertex for each loop $\lambda \in \mathcal{L}_X$, and adding an edge between two vertices if the corresponding loops share a dual face (if a loop bounds the same dual face twice, add a self-edge). Construct the loop complexes of types Y and Z correspondingly. The loop complexes of each type ($X/Y/Z$) are bipartite.

The complexity of a polycube is directly proportional to the number of loops in its loop structure. We can hence control the complexity of a polycube by adding or removing loops from its loop structure while maintaining validity.

4 THE ALGORITHM

In the following we describe our iterative algorithm that computes polycube layouts based on a valid loop structure. We say that a loop or a set of loops \mathcal{L} are *valid* for a given valid loop structure $\mathcal{S} = (\mathcal{L}_X, \mathcal{L}_Y, \mathcal{L}_Z)$ if $\mathcal{S} \cup \mathcal{L}$ or $\mathcal{S} \setminus \mathcal{L}$ is also a valid loop structure (adding or removing the loops in \mathcal{L} results in a valid loop structure).

Our algorithm is summarized in Algorithm 1. We initialize with the valid loop structure of a single cube (see Fig. 3 (a)). In Section 4.1 we describe how we compute loops and prove that we can find a valid loop to add within each zone of a valid loop structure. In Section 4.2 we explain how to realize a valid loop structure \mathcal{S} as a polycube layout P on the surface mesh \mathcal{M} . Finally, in Section 4.3 we show how to search efficiently for sets of valid loops that improve the quality of the final polycube layout. In the following, whenever we compute shortest paths, we do so with Dijkstra’s algorithm.

Algorithm 1 DualLoops

Input: a surface mesh \mathcal{M} of genus 0
Output: a valid polycube layout P on \mathcal{M}
 initialize loop structure \mathcal{S} on a single cube
while quality or complexity bounds are not met **do**
 add or remove valid loops to/from \mathcal{S}
 assess quality, possibly via polycube layout or hexahedral mesh
end while
 compute polycube layout P from \mathcal{S}
return P

4.1 Finding loops

As mentioned in the previous section, the exact location of each loop in the loop structure is irrelevant as long as the combinatorial criteria are satisfied. However, to actually compute with these loops efficiently, we do construct an explicit representation of each loop on the surface of the input mesh \mathcal{M} .

The conceptually simplest solution to represent loops on \mathcal{M} would be to follow the edges of \mathcal{M} . However, this approach has the drawback that we can “run out of space” between adjacent loops or might not be able to find a sequence of edges which travel in the preferred direction of the loop. Subdividing \mathcal{M} can mitigate these issues to a certain degree, however, this adds unnecessary complexity to the mesh and hence to all downstream computations.

Instead, we define a loop via a sequence of triangles in \mathcal{M} . This representation allows multiple parallel loops to share the same sequence of triangles. Since a loop is infinitely thin, a single triangle can be part of an infinite number of loops and hence the addition of loops does not restrict the domain. To implement this representation, we construct an *edge graph* G . G has a vertex for every edge in \mathcal{M} . Two vertices in G are connected if and only if the corresponding edges in \mathcal{M} share a triangle (see Fig. 5 (a)). A loop now corresponds to a cycle in the edge graph (see Fig. 5 (b), thicker edges indicate multiple loops). The combinatorial structure of nested and crossing loops induces a partial order on all loops; we can extend this partial order to a total order on each edge of the mesh \mathcal{M} . We realize the loop representation as an embedding on \mathcal{M} by distributing the loops evenly according to their order on each edge of \mathcal{M} (see Fig.5 (c)).

When a valid loop is added to the loop structure, it is always placed between existing loops of the same type. Since loops of the same type do not intersect, we can place the new loop between the existing loops in the order. Removing a loop does not change the order for the remaining loops.

Previous work [Campen et al. 2012; Livesu et al. 2020; Pietroni et al. 2016] has predominantly focused on paths guided by a cross field on the mesh surface to find loops. The idea is that a path starts at a vertex of the mesh and then follows the directional field around the mesh to return to its starting vertex to close the loop. This behaviour cannot be guaranteed and path might instead spiral around the mesh without ever closing a loop. Post-processing can remedy these issues, but success is not guaranteed.

In contrast, we show below how to direct and augment the edge graph G for each direction X , Y , and Z , such that finding a valid

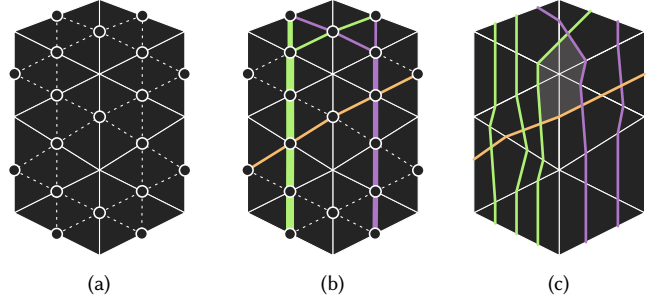


Fig. 5. (a) Edge graph G (dashed) on \mathcal{M} (solid), (b) loops represented as paths on G , (c) the embedding on \mathcal{M} . A dual face is indicated in gray.

loop in the respective direction corresponds to a shortest path computation in the augmented graph. By design, this shortest path computation is guaranteed to return a result.

In the following we focus on finding X -loops; we can find Y - and Z -loops in the same manner. We construct a graph G_X from the edge graph G as follows. First, we replace each edge in G by two directed edges and then assign a weight to each. To do so, we first embed G_X on \mathcal{M} by choosing the midpoint of each edge of \mathcal{M} as the location of the corresponding vertex of G_X . Each edge of G_X now lies on a triangular face of \mathcal{M} . Consider a directed edge $e = (u, v)$ of G_X . The edge e induces a *direction vector* $d(e)$ that is directed from u to v . Furthermore, we define a *normal vector* $n(e)$ for e which is the normal of the triangle of \mathcal{M} which contains e . Intuitively we would like to route an X -loop on edges of G_X that lie in a plane which is perpendicular to the X -axis. Most edges do not lie in such a plane, but the angle $\alpha_X(e)$ of the cross-product $d(e) \times n(e)$ with the X -axis measures how close they are. In fact, this angle also distinguishes between edges that travel clockwise or counter-clockwise around the X -axis; we choose to orient all loops in clockwise direction and hence prefer edges with low $\alpha_X(e)$.

As indicated above, we will use shortest path computations in a weighted version of G_X to find X -loops. Depending on the complexity of the loop structure we already computed and the current distortion induced by the resulting polycube layout, we might prefer long loops which follow the perpendicular direction very strictly over shorter loops that contain edges which deviate more substantially. To facilitate this, we introduce a parameter $1 \leq s \leq \infty$ which captures the *angular slack* of our desired cycle. The weight of each edge e of G_X is then set to $w_X(e) = \alpha_X(e)^s$.

To find a new loop starting at a vertex v , we consider all neighbors w of v . The shortest path from w to v concatenated with the directed edge (v, w) forms a cycle and hence a loop. The shortest cycle among these is the new loop starting at v . Note that it is unlikely that this loop consist of only two edges since a clockwise edge with a low weight has a counter-clockwise reverse with high weight.

We can easily adapt this process to find a loop within a single zone ζ , by pruning G_X to contain only those vertices that lie in or on the boundary of ζ . Zone ζ is bounded by at least one X -loop λ which is represented by a cycle c in G_X . The subgraph $G_X(\zeta)$ of G_X restricted to ζ is hence connected via its boundary cycle c .

THEOREM 4.1. *Given a valid loop structure \mathcal{S} and a zone ζ , there is a valid loop λ that lies within ζ .*

PROOF. Without loss of generality, we assume that ζ is an X -zone. Zone ζ is bounded by at least one X -loop λ which is represented by a cycle c in G_X . Consider now a second loop λ' which is also represented by c . We insert λ' in the order of loops next to λ inside of ζ . Loop λ' is a valid loop since

- (1) Trivially λ' does not intersect any loop of the same type.
- (2) Adding λ' does not introduce an intersection of three loops.
- (3) The dual faces between λ and λ' are of type (b) and (c) (refer to Fig. 3), which are valid.
- (4) Observe that the loop complex for a genus 0 polycube is in fact a tree, since cutting along a loop disconnects the polycube surface. We split the vertex representing λ into two vertices and add an edge between them. This operation does not introduce any cycles and hence the loop complex remains a tree and therefore bipartite.

□

4.2 From loop structure to polycube layout

We now show how to construct a polycube layout P from a valid loop structure \mathcal{S} . The layout P is valid by construction. As discussed before, a polycube layout for a mesh \mathcal{M} consists of patches on the surface of \mathcal{M} which are formed by adjacent triangles of \mathcal{M} . Each patch is defined by four *corners* which are vertices of \mathcal{M} . These four corners are connected by four non-intersecting paths composed from edges of \mathcal{M} . Each corner lies inside a dual face of \mathcal{M} . To construct a polycube layout we have to first find suitable vertex locations on \mathcal{M} to place the corners and then connect these corner via non-intersecting paths. Generally speaking, the set of patches of a polycube layout are considered “good” if they resemble the polycube: patches are flat, face into one of the principal directions, and form a grid pattern with aligned corners connected by straight paths. In practice, the quality of a polycube layout is often assessed via the quality of derived products, most notably, hexahedral meshes.

Let f be a dual face in the embedding of the dual loop structure \mathcal{S} on \mathcal{M} . Face f is the union of zero or more triangles of \mathcal{M} as well as zero or more convex sections cut from triangles via the embedding of the loops bounding f (see Fig. 5 (c)). We generate a set $C(f)$ of candidate corners for f . $C(f)$ contains all vertices of \mathcal{M} that lie inside f as well as the center points of all triangles and of all convex sections. Note that the latter points are not part of \mathcal{M} ; if we choose one of them to become the corner of f then we need to subdivide \mathcal{M} to include it. $C(f)$ contains always at least one point.

Each dual face corresponds to one of six possible combinatorial corner types. The corner type determines how many polycube faces of which principal direction meet in which way at this corner (see Fig. 3). We use the corner type when choosing a preliminary corner for f as follows. First, we naively label each triangle and convex section with a label $\pm X/\pm Y/\pm Z$, simply by rounding its normal to the closest direction. We then compute a center point for each set of triangles and convex sections that share the same label, weighted by area. We disregard those with a label that does not occur for the corner type of f . We choose as the preliminary corner for f the

point in $C(f)$ which minimizes the average Euclidean distance to the center points of the triangles and convex sections which have a label relevant for the corner type of f . Our experiments show that this preliminary corner separates the relevant directions well.

The preliminary corner tends to be a good choice for the individual face f . However, we also want to align corners. Each dual face belongs to exactly three zones, one for each principal direction. We compute an average x -coordinate x_{zone} from the preliminary corners of all faces that share the same X -zone. We compute the average y_{zone} and z_{zone} correspondingly. Finally, we choose the point in $C(f)$ which has the smallest Euclidean distance to the point $(x_{\text{zone}}, y_{\text{zone}}, z_{\text{zone}})$ as the corner of f .

It remains to compute non-intersecting paths connecting the corners. We do so in a simple incremental manner, which is efficient and produces paths of sufficient quality for our purposes. Let \mathcal{M}' be the mesh which has been subdivided to include all corners we chose in the previous step and let G' be the edge graph of \mathcal{M}' . We create a routing graph R from \mathcal{M}' and G' by connecting each vertex v of \mathcal{M}' to those vertices in G' that represent the “opposing” edge to v in each triangle that v is adjacent to.

We start with an arbitrary patch. We connect two of its adjacent corners with a shortest path in R . If this shortest path contains edges of G' then we subdivide \mathcal{M}' to include those edges and their vertices. Afterwards we update G' and R correspondingly. Then we remove all edges from R which belong to paths which we have already computed. We proceed in an incremental manner, working outwards from the initial patch according to a breadth-first search on the dual graph of the patches. This ensures that all corners that are yet to be connected by a path remain in the same connected component of R . Furthermore, all paths are disjoint by construction.

The patches form a valid polycube layout P . Every patch p has a corresponding label defined by the loop structure: $l(p)$. Each triangle t in patch p is assigned the same label $l(t) = l(p)$.

4.3 Evolutionary search algorithm

In the following we describe our algorithm that efficiently computes a high-quality loop structure \mathcal{S} for a mesh \mathcal{M} by iteratively adding and removing loops. Our algorithm is a simple type of evolutionary algorithm that uses only mutation and selection (no crossover). Every candidate solution in the population is guaranteed to be a valid loop structure. We use two types of quality metrics to guide our evolutionary algorithm. For the selection step we consider the entire solution (loop structure) and measure (an approximation of) the distortion of the resulting polycube layout. For the mutation step we do not choose completely random loops within all zones, but we use various quality criteria to find suitable loops to add to the loop structure. We find loops as described in Section 4.1; we detail the quality metrics below.

We first consider the quality of a single loop to be added to a loop structure \mathcal{S} . To do so, we need to introduce one more concept, namely the *angular defect* $\delta(v)$ of a vertex v in the mesh \mathcal{M} . We define this angular defect as $\delta(v) = 2\pi - C$, where C is the sum of angles (in radians) at v in incident triangles on \mathcal{M} . In a polycube, the vertices that have non-zero angular defect correspond to corners of type (a/d/e/f) (see Fig. 3). These corners are separated from each

other by loops. For a parameter ρ ($0 < \rho < 1$), we designate the top ρ fraction of vertices of \mathcal{M} based on absolute angular defect as *critical*. Two of our measures assess the ability of a loop to separate these critical vertices.

We define the following quality metrics for candidate loops:

Loop Length (maximize): The geometric length of the loop. Longer loops tend to capture more relevant features of the mesh and advance the complexity of the loop structure. This measure is particularly useful for finding good initial loops.

Loop Distribution (maximize): The distance to neighboring loops. For loops of type $X/Y/Z$, this distance is the absolute difference in the average $x/y/z$ -coordinate between two loops. Loops that are close together often capture the same features and may be redundant. Maximizing this distance ensures that the loops represent a wide range of features with minimal redundancy.

Critical Spread (minimize): The maximum distance between two critical vertices within a single zone. For zones of type $X/Y/Z$, this distance is measured as the absolute difference between $x/y/z$ -coordinates. Loops that separate distant critical vertices within the same zone are preferred.

Critical Count (minimize): The maximum number of critical vertices in a single zone. This measure aims to distribute critical vertices across different zones.

To assess the quality of an entire solution, we use a combination of two metrics that capture the distortion of the resulting polycube layout P (computed as described in Sec. 4.2): the *triangle alignment* and the *patch orthogonality*. For a triangle t in \mathcal{M} we can determine its label $l(t)$ from P . The *triangle alignment* of t in P is computed as $a(t, P) = 1 - (1 + e^{2\pi - 4a})^{-1}$, where a is the angle in radians between the normal $n(t)$ and the label $l(t)$ of the triangle t . The triangle alignment score lies in the range $[0, 1]$, where 1 implies perfect alignment. Note that for angles a smaller than 1 radian (approx. 55 degrees) the score lies above 0.9, which avoids heavily penalizing triangles that cannot align well with any principal axis.

For a single patch p in the polycube layout P , we can easily determine its 4 corners c_1, \dots, c_4 (in clockwise order). For a corner c_i we consider the angle $a(c_i)$ between the vectors $c_{i+1} - c_i$ and $c_{i-1} - c_i$ (looping around where necessary). The *orthogonality* of a single corner c_i is computed as $\sin^2(a(c_i))$. The *patch orthogonality* $r(p)$ of a patch p is the minimum orthogonality of all its corners (the value associated with the worst corner). Note that $r(p)$ is again a value in the range $[0, 1]$.

Finally, we can compute the *accuracy* $\text{acc}(\mathcal{M}, P)$ of a polycube layout P of a given mesh $\mathcal{M} = (V, T)$ by taking a weighted sum of the metrics above:

$$\text{acc}(\mathcal{M}, P) = \kappa \sum_{t \in T} \left(a(t, P) \cdot \frac{A(t)}{A(\mathcal{M})} \right) + (1 - \kappa) \sum_{p \in P} \left(r(p) \cdot \frac{A(p)}{A(\mathcal{M})} \right)$$

where κ is a parameter (we use $\kappa = 0.9$). The function $A(\dots)$ computes the area of a triangle, patch, or mesh.

Our evolutionary algorithm now works as follows. We first initialize a single solution by creating a loop structure with one loop of each type. This loop structure is obtained by trying all permutations of $\{X, Y, Z\}$ and adding loops in that order based on the loop length quality criterion. Only the best result is used as starting solution.

In the remainder of the algorithm we maintain a population of at most N solutions. In every iteration we generate N' offspring solutions by choosing a random parent solution and mutating the solution as follows. We first try to add n_l loops. For each loop we randomly choose a zone ζ , an angular slack $2.5 \leq s \leq 7.5$, a quality criteria $q \in \{\text{loop length, loop distribution, critical spread, critical count}\}$, and $0.01 \leq \rho \leq 0.5$. We then randomly generate n_c candidate loops in ζ using angular slack s by randomly selecting starting vertices in ζ and using the approach of Sec. 4.1 (only keeping valid loops). The best scoring loop among the n_c candidates according to the quality criterion q is added to the loop structure. After adding loops, we also attempt to remove randomly selected loops n_r times. We remove a loop only if the resulting loop structure is still valid and the accuracy of the entire solution does not decrease. Finally, among all N' generated solutions (including the N parent solutions), we pick the N best solutions in terms of accuracy for the next iteration of the algorithm. If the accuracy of the best solution does not improve by some threshold τ between generations, then we terminate the algorithm and output the best solution.

5 RESULTS

We implemented our DualLoops algorithm¹ and evaluated it on a set of diverse input meshes.² We also compared our results to two state-of-the-art methods: PolyCut³ by [Livesu et al. 2013] and EvoCube⁴ by [Dumery et al. 2022]. To be as fair as possible in the comparison, we used the polycube labelings computed by all three methods (PolyCut, EvoCube, and our DualLoops) as input for RobustPolycube⁵ by [Protais et al. 2022] to compute polycube maps and hexahedral meshes. As a result, the values for PolyCut and EvoCube differ in places from those reported in earlier papers, where a different downstream pipeline was used. For PolyCut, EvoCube, and RobustPolycube we used default parameters; for our method we used $N = 2$, $N' = 8$, $n_l = 10$, $n_r = 15$, $n_c = 200$, and $\tau = 0.001$.

For our comparison we generated polycube labelings from all three algorithms for 24 input meshes. As it is common, we measured the quality of the polycube labelings via the quality of the derived polycube maps and hexahedral meshes. The results are summarized in Table 1. When we refer to an input model, we use its common name and the number of triangular faces (in brackets). Visual results are showcased in Fig. 6 and Fig. 7. The hexahedral meshes are visualized using HexaLab⁶ by [Bracci et al. 2019], with the hex quality color setting showing the Scaled Jacobian of the cells.

The evaluation of the polycube maps involves computing area and angular distortion [Dumery et al. 2022; Floater and Hormann 2005; Livesu et al. 2013; Tarini et al. 2004]. The evaluation of the hexahedral meshes involves computing cell quality via the scaled Jacobian [Pietroni et al. 2022], vertex quality via vertex irregularity [Pietroni et al. 2022], and geometric fidelity using the Hausdorff distance [Fang et al. 2016; Guo et al. 2020; Huang et al. 2014]. For reproducibility, we briefly explain how these metrics are computed.

¹ github.com/maximsnoep/Polycube-Layouts-via-Iterative-Dual-Loops

² github.com/maximsnoep/manimeshes

³ cs.ubc.ca/labs/imager/tr/2013/polycut

⁴ github.com/LIHPC-Computational-Geometry/evocube

⁵ github.com/fprotais/robustPolycube

⁶ hexalab.net

| | D_{area} | D_{angle} | #hexes | SJ_{min} | SJ_{avg} | %irr | $\overline{\text{HD}}$ |
|---|-------------------|--------------------|--------|-------------------|-------------------|------|------------------------|
| blub (14.208) | | | | | | | |
| PC | 1,759 | 2,023 | 23.022 | -0,992 | 0,842 | 2,8 | 4,195 |
| EC | 1,919 | 3,229 | 9.359 | -0,901 | 0,807 | 4,0 | 8,963 |
| DL | 3,473 | 2,580 | 17.016 | 0,033 | 0,886 | 4,7 | 3,168 |
| bunny (6.598) | | | | | | | |
| PC | 1,210 | 1,216 | 10.813 | 0,061 | 0,900 | 3,5 | 2,806 |
| EC | 1,260 | 1,439 | 10.535 | 0,029 | 0,902 | 4,6 | 12,837 |
| DL | 1,574 | 1,698 | 17.210 | 0,112 | 0,928 | 4,5 | 5,082 |
| igea (10.000) | | | | | | | |
| PC | 1,281 | 1,722 | 36.656 | 0,024 | 0,911 | 1,2 | 1,884 |
| EC | 1,398 | 1,800 | 17.442 | -0,921 | 0,885 | 1,9 | 2,278 |
| DL | 2,355 | 2,561 | 18.448 | 0,064 | 0,933 | 1,7 | 1,794 |
| moai (20.000) | | | | | | | |
| PC | 1,290 | 1,294 | 66.536 | 0,053 | 0,955 | 0,9 | 1,213 |
| EC | 1,190 | 1,303 | 51.038 | 0,060 | 0,959 | 1,4 | 1,870 |
| DL | 1,625 | 3,283 | 55.292 | 0,085 | 0,960 | 0,9 | 1,296 |
| sphinx (21.212) | | | | | | | |
| PC | 1,289 | 1,430 | 53.534 | 0,067 | 0,947 | 1,7 | 1,542 |
| EC | 1,369 | 1,589 | 49.816 | 0,041 | 0,940 | 2,0 | 2,343 |
| DL | 2,100 | 2,906 | 53.820 | 0,079 | 0,936 | 1,3 | 1,497 |
| venus (21.744) | | | | | | | |
| PC | 2,280 | 1,442 | 56.386 | 0,108 | 0,949 | 1,1 | 1,453 |
| EC | 1,472 | 1,474 | 52.116 | 0,195 | 0,944 | 1,1 | 2,481 |
| DL | 1,339 | 1,280 | 65.928 | 0,036 | 0,951 | 1,2 | 0,998 |
| average over whole dataset (24 inputs) | | | | | | | |
| PC | 1,463 | 1,591 | - | -0,032 | 0,897 | 3,8 | 2,573 |
| EC | 1,503 | 1,833 | - | -0,004 | 0,899 | 4,6 | 5,590 |
| DL | 1,981 | 3,338 | - | 0,092 | 0,915 | 4,0 | 4,302 |

Table 1. Comparison of polycube maps and hexahedral meshes generated via the RobustPolycube pipeline [Protais et al. 2022], using the polycube labelings from PolyCut (PC) [Livesu et al. 2013], EvoCube (EC) [Dumery et al. 2022], and our method (DL).

Consider the mapping $\phi : \mathcal{M} \rightarrow \mathcal{Q}$, which linearly maps the triangles of surface mesh \mathcal{M} to the polycube \mathcal{Q} . Area and angular distortion are derived from the singular values σ_1 and σ_2 of the Jacobian matrix $J_{\phi|t}$ at each triangle t . The overall distortion of the polycube map is obtained by averaging these values across all triangles, weighted by their area in the polycube domain.

$$D_{\text{area}}(\phi|t) = \sigma_1\sigma_2 + \frac{1}{\sigma_1\sigma_2}, \quad D_{\text{angle}}(\phi|t) = \frac{\sigma_1}{\sigma_2} + \frac{\sigma_2}{\sigma_1}$$

The Scaled Jacobian (SJ) of a hexahedral cell h that is part of a hexahedral mesh \mathcal{H} is the minimum of the Jacobian determinants at each vertex of h , normalized by the lengths of the three adjacent edges (e_1 , e_2 , and e_3):

$$SJ(h) = \min_{v \in h} \left(\frac{\det J(v)}{|e_1| \cdot |e_2| \cdot |e_3|} \right)$$

We report on the minimum and average SJ across all cells in \mathcal{H} . Hexahedral meshes with cells with $SJ(h) < 0$ (inverted or degenerate cells) are typically unusable for simulation.

We measure mesh irregularity (%irr) via the percentage of irregular vertices. A vertex of a hexahedral mesh is *regular* if it is adjacent to 2, 4, or 8 hexahedral cells, and *irregular* otherwise. Similarity between the input model \mathcal{M} and the surface of hexahedral mesh \mathcal{H} is measured using the symmetric Hausdorff distance $\overline{\text{HD}}$. We normalize the Hausdorff distance by dividing it by the length of the diagonal of the axis-aligned bounding box encompassing \mathcal{M} (the scale of \mathcal{M}). In Table 1 we further multiply the Hausdorff distance by 100 to facilitate a concise presentation of the results.

Recall that our method is guaranteed to always return a valid polycube (labeling). Hence we did not include any measures of (pseudo-)validity in our results. Furthermore, our algorithm regularly outperforms the others in terms of the Scaled Jacobian (SJ) and overall similarity, and generally performs on par with both. We can observe that our algorithm finds comparatively straight paths that delimit areas of the same orientation in the polycube labeling (see the boundaries of the red, blue, and beige regions in Fig. 6). We believe that this is due to the alignment of corners in their three $X/Y/Z$ -zones. Our DualLoops algorithm does particularly well on “rough” and complex models such as igea (Fig. 6(c)), since our iterative approach tends to pick up on the global shape first and does not get side-tracked by local features. On the flip-side, our algorithm sometimes fails to capture features well that are not aligned with any of the principal directions, such as the horns of the goat head (Fig. 7(d)). Such cases have a significant negative impact on our average similarity score. Finally, when we investigated the scores on area and angular distortion in detail, we saw that they were dominated by outliers. They also do not appear to have a predictive value for the quality of derived hexahedral meshes.

6 CONCLUSION

We introduced a new algorithm which is guaranteed to return a valid polycube layout for 3D models of genus 0. The algorithm uses the dual structure of polycubes and supports iterative refinement. Our experiments show that our algorithm is effective. Both the models used in our evaluation and our source code are openly available.

One major limitation of our current approach is its restriction to models of genus 0. While we do believe that an extension to higher genus models is possible, there are several challenges to overcome on the way. First of all, we need to find a set of initial loops on the input mesh which correspond to a valid polycube of the correct genus. Second, the combinatorial characterization of a valid loop structure currently exists only for polycubes of genus 0 and we need to find corresponding conditions for higher genus polycubes.

Last but not least, we believe that manual interaction could significantly enhance the results of our method. Our approach has a natural compatibility with manual intervention, since we can choose zones and starting vertices for loop additions freely. Furthermore, our algorithm can easily validate loops suggested by a user. In the future we hence plan to explore possibilities for human interaction, such as, for example, the loop drawing methodology demonstrated in [Campen and Kobbelt 2014].

REFERENCES

- Markus Baumeister and Leif Kobbelt. 2023. How close is a quad mesh to a polycube? *Computational Geometry* 111, Article 101978 (April 2023), 22 pages. <https://doi.org/10.1016/j.comgeo.2022.101978>
- Therese Biedl and Burkay Genc. 2004. When can a graph form an orthogonal polyhedron?. In *Proceedings of the 16th Canadian Conference on Computational Geometry* (Montreal, Quebec, Canada) (CCCG '04). 53–56. <http://www.cccg.ca/proceedings/2004/15.pdf>
- Matteo Bracci, Marco Tarini, Nico Pietroni, Marco Livesu, and Paolo Cignoni. 2019. HexaLab.net: An online viewer for hexahedral meshes. *Computer-Aided Design* 110 (2019), 24–36. <https://doi.org/10.1016/j.cad.2018.12.003>
- Marcel Campen, David Bommes, and Leif Kobbelt. 2012. Dual Loops Meshing: Quality Quad Layouts on Manifolds. *ACM Transactions on Graphics* 31, 4, Article 110 (July 2012), 11 pages. <https://doi.org/10.1145/2185520.2185606>
- Marcel Campen and Leif Kobbelt. 2014. Dual strip weaving: interactive design of quad layouts using elastica strips. *ACM Transactions on Graphics* 33, 6, Article 183 (Nov. 2014), 10 pages. <https://doi.org/10.1145/2661229.2661236>
- Gianmarco Cherchi, Marco Livesu, and Riccardo Scateni. 2016. Polycube Simplification for Coarse Layouts of Surfaces and Volumes. *Computer Graphics Forum* 35, 5 (Aug. 2016), 11–20. <https://doi.org/10.1111/cgf.12959>
- Corentin Dumery, François Protais, Sébastien Mestrallet, Christophe Bourcier, and Franck Ledoux. 2022. Evocube: A Genetic Labelling Framework for Polycube-Maps. *Computer Graphics Forum* 41, 6 (Sept. 2022), 467–479. <https://doi.org/10.1111/cgf.14649>
- David Eppstein and Elena Mumford. 2010. Steinitz Theorems for Orthogonal Polyhedra. In *Proceedings of the Twenty-Sixth Annual Symposium on Computational Geometry* (Snowbird, Utah, USA) (SoCG '10). Association for Computing Machinery, New York, NY, USA, 429–438. <https://doi.org/10.1145/1810959.1811030>
- Xianzhong Fang, Weiwei Xu, Hujun Bao, and Jin Huang. 2016. All-Hex Meshing Using Closed-Form Induced Polycube. *ACM Transactions on Graphics* 35, 4, Article 124 (July 2016), 9 pages. <https://doi.org/10.1145/2897824.2925957>
- Michael S. Floater and Kai Hormann. 2005. Surface Parameterization: a Tutorial and Survey. In *Advances in Multiresolution for Geometric Modelling*. Springer Berlin Heidelberg, Berlin, Heidelberg, 157–186.
- Xiao-Ming Fu, Chong-Yang Bai, and Yang Liu. 2016. Efficient Volumetric PolyCube-Map Construction. *Computer Graphics Forum* 35, 7 (Oct. 2016), 97–106. <https://doi.org/10.1111/cgf.13007>
- James Gregson, Alla Sheffer, and Eugene Zhang. 2011. All-Hex Mesh Generation via Volumetric Polycube Deformation. *Computer Graphics Forum* 30, 5 (Aug. 2011), 1407–1416. <https://doi.org/10.1111/j.1467-8659.2011.02015.x>
- Hao-Xiang Guo, Xiaohan Liu, Dong-Ming Yan, and Yang Liu. 2020. Cut-Enhanced PolyCube-Maps for Feature-Aware All-Hex Meshing. *ACM Transactions on Graphics* 39, 4, Article 106 (Aug. 2020), 14 pages. <https://doi.org/10.1145/3386569.3392378>
- Ying He, Hongyu Wang, Chi-Wing Fu, and Hong Qin. 2009. A divide-and-conquer approach for automatic polycube map construction. *Computers & Graphics* 33, 3 (June 2009), 369–380. <https://doi.org/10.1016/j.cag.2009.03.024>
- Jin Huang, Tengfei Jiang, Zeyun Shi, Yiyang Tong, Hujun Bao, and Mathieu Desbrun. 2014. ℓ_1 -Based Construction of Polycube Maps from Complex Shapes. *ACM Transactions on Graphics* 33, 3, Article 25 (June 2014), 11 pages. <https://doi.org/10.1145/2602141>
- Juncong Lin, Xiaogang Jin, Zhengwen Fan, and Charlie C. L. Wang. 2008. Automatic Polycube-Maps. In *Proceedings of the 5th International Conference on Advances in Geometric Modeling and Processing* (Hangzhou, China) (GMP'08). Springer-Verlag, Berlin, Heidelberg, 3–16. https://doi.org/10.1007/978-3-540-79246-8_1
- Marco Livesu, Nico Pietroni, Enrico Puppo, Alla Sheffer, and Paolo Cignoni. 2020. LoopyCuts: Practical Feature-Preserving Block Decomposition for Strongly Hex-Dominant Meshing. *ACM Transactions on Graphics* 39, 4, Article 121 (Aug. 2020), 17 pages. <https://doi.org/10.1145/3386569.3392472>
- Marco Livesu, Nicholas Vining, Alla Sheffer, James Gregson, and Riccardo Scateni. 2013. Polycut: Monotone Graph-Cuts for Polycube Base-Complex Construction. *ACM Transactions on Graphics* 32, 6, Article 171 (Nov. 2013), 12 pages. <https://doi.org/10.1145/2508363.2508388>
- Manish Mandad, Ruizhi Chen, David Bommes, and Marcel Campen. 2022. Intrinsic mixed-integer polycubes for hexahedral meshing. *Computer Aided Geometric Design* 94, Article 102078 (March 2022), 15 pages. <https://doi.org/10.1016/j.cagd.2022.102078>
- Sébastien Mestrallet, François Protais, Christophe Bourcier, and Franck Ledoux. 2023. Limits and prospects of polycube labelings. In *SIAM International Meshing Roundtable Workshop 2023* (Amsterdam, The Netherlands) (SIAM IMR23). 5 pages. <https://internationalmeshingroundtable.com/assets/research-notes/imr31/2012-comp.pdf>
- Nico Pietroni, Marco Campen, Alla Sheffer, Gianmarco Cherchi, David Bommes, Xifeng Gao, Riccardo Scateni, Franck Ledoux, Jean Remacle, and Marco Livesu. 2022. Hex-Mesh Generation and Processing: A Survey. *ACM Transactions on Graphics* 42, 2, Article 16 (Oct. 2022), 44 pages. <https://doi.org/10.1145/3554920>
- Nico Pietroni, Enrico Puppo, Giorgio Marcias, Roberto Scopigno, and Paolo Cignoni. 2016. Tracing Field-Coherent Quad Layouts. *Computer Graphics Forum* 35, 7 (Oct. 2016), 485–496. <https://doi.org/10.1111/cgf.13045>
- François Protais, Maxence Reberol, Nicolas Ray, Ettiène Corman, Franck Ledoux, and Dmitry Sokolov. 2022. Robust Quantization for Polycube Maps. *Computer-Aided Design* 150, Article 103321 (Sept. 2022), 11 pages. <https://doi.org/10.1016/j.cad.2022.103321>
- Dmitry Sokolov and Nicolas Ray. 2015. *Fixing normal constraints for generation of polycubes*. Research Report. LORIA. <https://inria.hal.science/hal-01211408>
- Marco Tarini, Kai Hormann, Paolo Cignoni, and Claudio Montani. 2004. Polycube-Maps. *ACM Transactions on Graphics* 23, 3 (Aug. 2004), 853–860. <https://doi.org/10.1145/1015706.1015810>
- Shenghua Wan, Zhao Yin, Kang Zhang, Hongchao Zhang, and Xin Li. 2011. A topology-preserving optimization algorithm for polycube mapping. *Computers & Graphics* 35, 3 (June 2011), 639–649. <https://doi.org/10.1016/j.cag.2011.03.018>
- Hongyu Wang, Ying He, Xin Li, Xianfeng Gu, and Hong Qin. 2008. Polycube Splines. *Computer-Aided Design* 40, 6 (June 2008), 721–733. <https://doi.org/10.1016/j.cad.2008.01.012>
- Yang Yang, Xiao-Ming Fu, and Ligang Liu. 2019. Computing Surface PolyCube-Maps by Constrained Voxelization. *Computer Graphics Forum* 38, 7 (Nov. 2019), 299–309. <https://doi.org/10.1111/cgf.13838>
- Wuyi Yu, Kang Zhang, Shenghua Wan, and Xin Li. 2014. Optimizing polycube domain construction for hexahedral remeshing. *Computer-Aided Design* 46 (Jan. 2014), 58–68. <https://doi.org/10.1016/j.cad.2013.08.018>
- Hui Zhao, Xuan Li, Wencheng Wang, Xiaoling Wang, Shaodong Wang, Na Lei, and Xiangfeng Gu. 2019. Polycube Shape Space. *Computer Graphics Forum* 38, 7 (Nov. 2019), 311–322. <https://doi.org/10.1111/cgf.13839>

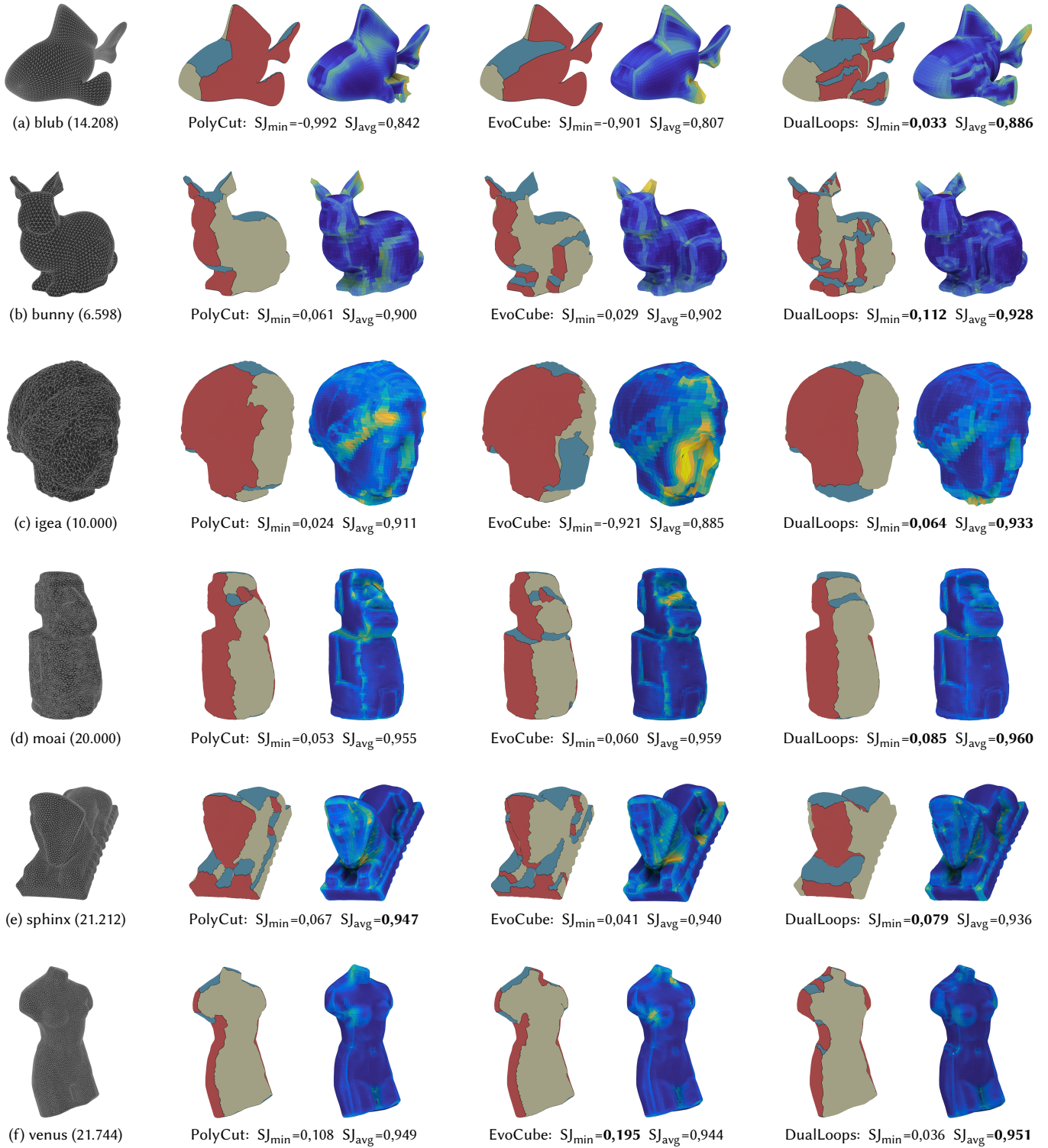


Fig. 6. Comparison of the three methods PolyCut [Livesu et al. 2013], EvoCube [Dumery et al. 2022], and our method DualLoops, on the models featured in Table 1. We show the input mesh, polycube labelings, and resulting hexahedral meshes, including the values for SJ_{min} , SJ_{avg} . The best values per input in bold.

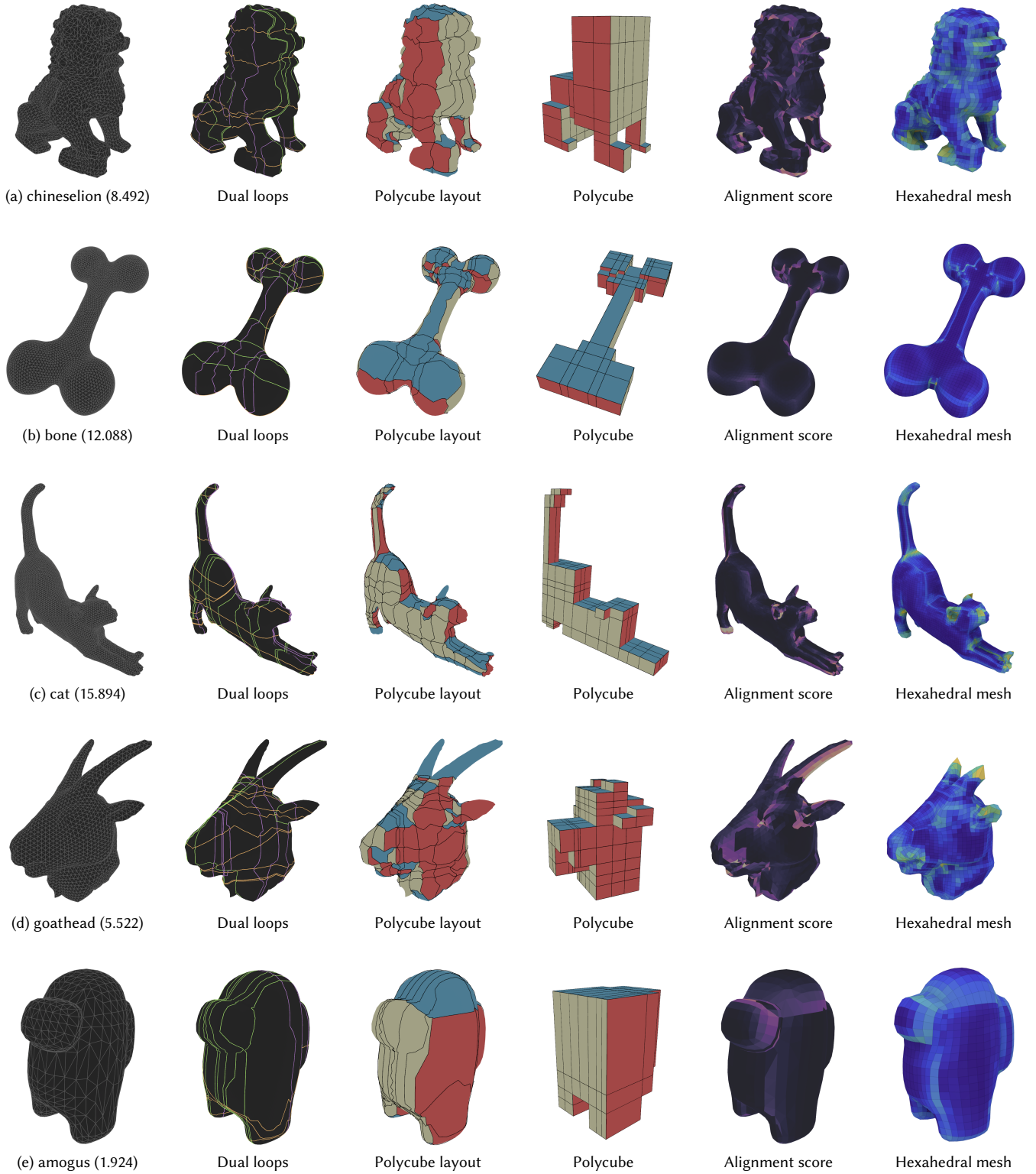


Fig. 7. Showcase of results generated by our DualLoops algorithm, illustrating the transformation from loop structure to polycube layout. Alignment of triangles is visualized via lightness from light (low alignment) to dark (high alignment). Hexahedral mesh computed as per [Protais et al. 2022].